Dynamic Underwater Glider Network for Environmental Field Estimation

R. GRASSO
P. BRACA, Member IEEE
NATO STO CMRE
Spezia, Italy

S. FORTUNATI, Member IEEE
F. GINI, Fellow, IEEE
M. S. GRECO, Fellow, IEEE
University of Pisa
Pisa, Italy

A coordinated dynamic sensor network of autonomous underwater gliders to estimate three-dimensional time-varying environmental fields is proposed and tested. Integration with a network of surface relay nodes and asynchronous consensus are used to distribute local information and achieve the global field estimate. Field spatial sparsity is considered, and field samples are acquired by compressive sensing devices. Tests on simulated and real data demonstrate the feasibility of the approach with relative error performance within 10%.

Manuscript received December 12, 2014; revised May 29, 2015; released for publication September 1, 2015.

DOI. No. 10.1109/TAES.2015.140935.

Refereeing of this contribution was handled by S. Marano.

This work has been funded by the NATO Allied Command Transformation (NATO-ACT) under the project ACT000405, Environmental Knowledge and Operational Effectiveness–Decisions in Uncertain Ocean Environments (EKOE-DUOE).

Authors' addresses: R. Grasso, P. Braca, NATO STO CMRE, Viale San Bartolomeo 400, La Spezia, Italy; S. Fortunati, F. Gini, M, S. Greco, Dipartimento di Ingegneria dell'Informazione, University of Pisa, via G. Caruso 16, 56122 Pisa, Italy, E-mail: (grasso@cmre.nato.int).

I. INTRODUCTION

The advent and improvement of autonomous underwater vehicle technology open wide new perspectives on sampling the ocean efficiently and persistently at feasible costs [1, 2]. In particular, the autonomous capability of robotic-sampling networks, able to satisfy in real-time prescribed requirements, exhibits high-quality ocean field estimation and forecast. At the same time, this kind of networks poses new challenging problems regarding the managing and the automatic control of such networks [3, 4]. Recent advances in distributed statistical signal-processing techniques related to the control and the inference in dynamic sensor networks provide a robust theoretical framework to tackle several challenges [5–9]. Furthermore, this paradigm of autonomous network of vehicles permits the ocean sampling with a minimum amount of human supervision.

This work describes an approach for optimally estimating slowly varying environmental spatial fields in a distributed fashion by a fleet of autonomous underwater vehicles (agents), integrated with a network of relay nodes (RNs). The system architecture allows all the agents and RNs to converge to the optimal estimated field. These characteristics are suitable, in particular, for the control of a network of underwater vehicles, where each agent of the network can communicate sporadically with one or more RNs (see Fig. 1).

We focus on the case of an underwater network of agents, such as gliders [1], that sporadically emerge to perform satellite or radio communications.

Underwater communications are not used because the glider agents considered in this work, mainly for technological limits (vehicle size and energy budget), are not equipped with an acoustic modem (transmit/receive). The agents do not directly communicate each other, neither underwater nor at surface. Communications are only asynchronous at the surface between agents and a network of RNs that is reachable by a vehicle with high probability through satellite/radio links when it is at the surface. Synchronous communications at surface among agents are unfeasible because it is difficult to synchronize the surfacing phase of the vehicles. The sensor network envisioned in this work has a wide geographic extension to cover large areas on the order of tens/hundreds of kilometers. In order to exchange information frequently, directly between agents, by using underwater communications, the communication range should be sufficiently big in order to avoid the vehicles having to communicate only when they are in proximity of each other. Considering the typical extension of the surveyed area and the slow speed of the vehicles (nominally 0.6 m/s), short communication ranges will make the information exchange very poor, degrading the overall performance of the system. Again, for the moment, a long-distance underwater communication capability goes beyond the technological limits of the considered class of vehicles. Nevertheless, the distributed estimation

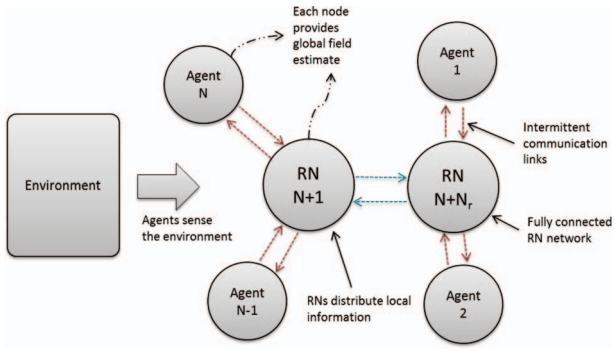

Fig. 1. Sensor network structure.

algorithm and network control proposed in this work is still valid, with minor changes, in case technology allows for different communication architectures, such as an ad hoc network of underwater nodes where gliders pass on information to each other.

The RN acts as an information gateway to asynchronously distribute the local information collected by a sensor to all the other sensors. The global estimation of the spatial field is, in this way, iteratively computed and somehow shared by all the nodes of the network. The estimated field can be retrieved by interrogating a node when this is reachable by the user. The information diffusion is based on the consensus protocol among sensors and the RN(s) [7, 10–12].

The RNs supporting the agent network of underwater gliders can include a single remote command-and-control center communicating with gliders at surface through a satellite link (like Iridium) [1], oceanographic fixed surface buoys, surface vehicles (like wave gliders) [13, 14], and/or an oceanographic mother ship all connected by satellite and/or radio links or a combination of the previous options. Normally, these surface assets are deployed during oceanographic campaigns so that the additional cost of configuring them as a network of RNs is negligible.

The spatial field of interest is assumed to be constant in time or slowly time varying. Moreover, we also consider the case in which the field is spatially sparse, i.e., the field can be represented by a number of informative components that is lower than the total number of dictionary base functions used to represent it. The estimation algorithm is based on a sparsity-aware Kalman filter (SA-KF) [15, 16] to refine the solution by taking into account the field sparsity constraints. The sensors are equipped with a compressive sensing (CS) device [17] to compress the collected information directly at the sampling stage. In this way, the sensors can operate at a lower sampling rate than the original sensor rate, preserving information and simplifying the sampling hardware on the side of the analog front end [17].

The network-sampling strategy is adaptive. In particular, the path of an agent of the network is optimized in such a way that the agents are forced to move into the most informative regions, e.g., see [9]. In other words, the measurements are collected in those areas where the estimate is more inaccurate.

The proposed architecture can be applied to map spatial fields for any measureable environmental parameter such as seawater temperature and optical properties, acoustic noise distribution, and pollutant concentration. Moreover, with some suitable modifications, the system can become a target grid tracker as proposed in [15, 16], a distributed device for herding activity in intelligence, or border security applications as suggested in [18].

The architecture can find use especially in the case of large-scale networks of autonomous underwater vehicles like gliders [1]. These vehicles typically perform underwater missions covering large areas and for long periods of time (even months). They can communicate to a command-and-control center through a satellite link (or a radio link in the proximity of the coast, mother ships, and/or surface vehicles) only when at sea surface and cannot communicate underwater with other vehicles or gateways through an acoustic link at very long range due to energy budget and communication equipment constraints. They form a multipayload platform carrying onboard several scientific sensors at the same time such as conductivity, temperature and depth sensors, seawater optical parameter sensors, and acoustic hydrophones, thus implying a great accumulation of data in the vehicle storage system.

This work follows the seminal papers [18, 19] on spatial field-distributed estimation by dynamic sensor networks in a centralized as well as decentralized way for the static and dynamic cases. The protocols proposed in these works suppose that neighboring agents can communicate each other continuously. These papers do not take into account networks with intermittent communication links and the sparsity of the spatial field. Moreover, sensors work at the Nyquist rate and are not equipped with a CS device. The SA-KF was introduced in [15, 16], where the authors propose a grid-tracking system taking advantage of the inherent sparsity of the surveillance scene (that is usually characterized by a number of targets that is much lower than the total number of grid cells). The work deals with static sensors, and the authors do not suggest any application to dynamic sensor networks.

The novel contribution of this paper consists in the design and the application of an adaptive dynamic network for three-dimensional (3D) ocean field estimation in a distributed way by a fleet of underwater autonomous gliders. In particular, the originality of this work is in the combination of advanced well-known techniques in sensor networks, distributed inference, dynamic network control, and sparse sampling, and in their use in an oceanographic application that is challenging. The design solves the sporadic and asynchronous communication-limiting factors, promotes a parsimonious and compact field representation by introducing spatial sparsity constraints, and directly compresses the acquired information at the sampling stage by using CS devices.

The paper aims at evaluating the performance of the system for specific scenarios. The scenarios reported here

are based on simulated 3D static and dynamic spatially sparse fields and on a real nonsparse oceanographic forecast model of the seawater temperature, i.e., the Navy Coastal Ocean Model (NCOM) [20]. The achieved mean steady-state relative error between the estimated and the true field is within 10%.

This paper is organized as follows. Section II provides the overview of the system. In particular, the field decomposition is first introduced; the field estimation algorithm based on a centralized KF architecture is described, and the CS sensor device model that is used to modify the original KF measurement equation is specified; and the subsections on SA-KF, agent control law, and kinematic model of underwater autonomous glider close Section II. In Section III, the centralized architecture is distributed and the consensus protocol is detailed. Section IV provides simulation results while Section V ends the paper drawing conclusions and highlighting future work.

II. CENTRALIZED ESTIMATION

This section provides an overview of the centralized field estimation algorithm. Methods to promote the sparsity in the estimation at the local nodes will also be introduced. The consensus protocol will be detailed later in Section III. The estimation procedure relies on the expansion of the spatial field on a basis of known spatial functions, weighted by unknown coefficients that are in general time variant. The spatial field to be estimated can be written as [18]:

$$g(\mathbf{r};t) = \sum_{j=1}^{L} c_j(t)\psi_j(\mathbf{r}) = \Psi(\mathbf{r})\mathbf{c}(t) \tag{1}$$

where $\mathbf{r}$ is the spatial position vector in the region of interest (for instance 2D or 3D, in a Cartesian reference system), $\mathbf{c} = [c_1, \ldots, c_L]^T$, c_j is the jth coefficient, $\psi_j(\mathbf{r})$ is the jth base function, and L is the total number of base functions. For the sake of clarity, from now on, the time variable t is dropped from the coefficient expressions. Given the base of spatial functions, $\Psi(\mathbf{r}) = [\psi_1(\mathbf{r}), \ldots, \psi_L(\mathbf{r})]$, the problem of estimating the scalar field from the sensor measurements is equivalent to estimate the coefficient vector $\mathbf{c}$.

We assume here that the coefficient vector $\mathbf{c}$ is sparse, i.e., the coefficient vector has $K \ll L$ nonzero components whose amplitude and support are unknown. In this case, the vector $\mathbf{c}$ can be conveniently estimated using algorithms that take into account its sparsity. Here, we use a SA-KF, as suggested in [15, 16]. Moreover, the network agents considered in this work are equipped with a sparse sensing acquisition device such as the random demodulator (RD) [17]. The coefficient vector can be estimated sequentially at a sampling rate lower than the Nyquist limit by including in the KF measurement equation the sparse device model.

The following subsections will detail the estimation algorithm in various forms. In particular, the centralized model is first introduced, together with the coordinated network control. The CS version of the algorithm is described, introducing first the RD measurement equation and then the SA-KF. A description of the agent used in simulation tests is also provided, including the kinematic and the operational and communication constraints.

A. Centralized Estimation

Centralized coefficient estimation is based on a network of agents that communicate to a fusion center (FC) their local field estimates at each time step k. The FC processes the local estimates by averaging them to obtain the global field estimate. The centralized algorithm detailed here is not feasible for a glider network because it would require local estimates available at the FC at each time step. This is not possible because the vehicles cannot communicate acoustically underwater with the FC, but only when at surface, typically every 1 to 3 h, by a satellite/radio link. The centralized system is then an ideal system that is used to compare the consensus-based distributed solution detailed in Section III.

The estimation-level fusion (similar to track-to-track fusion as in [21, 22]), rather than the KF centralized solution that fuses the sensor measurements [18], has been chosen for several reasons. The fusion algorithm used here is optimum in the minimum mean square error and maximum likelihood sense considering the sensors estimates as independent [21–23]. Because this hypothesis is not always true, the FC processor is in general suboptimal, but with the advantage of reducing complexity. The FC (as well as the RNs in the consensus algorithm as detailed in Section III) does not explicitly promote sparsity. Instead, the sparsity is promoted at the agent local level (see sub-Sections IIB and IIC), and the sensor estimates are fused in the FC (or in the RNs) similarly to [24] in which a pool of sparse solutions are averaged in order to improve the final estimate. The fused estimate is then fed back to the sensors to reinitialize the local estimates. The sensors indirectly share information among them, and, because the agents share the same field model, the local estimates converge in terms of support and amplitude to the true global state vector after a transitory phase. Moreover, being the distributed consensus algorithm based on the fusion of local agent estimates as detailed in Section III, the comparison with the centralized solution is more consistent and straightforward. The comparison with a measurement-level centralized solution is also possible, and it can be a further topic for future work.

Compared to a solution in which the agents exchange their measurements with the FC (or the RNs) and the control of the agent network is centralized as in [18], the approach here followed, based on estimation-level fusion and local agent control, has a higher communication overhead. However, it makes the integration of new agents in the network more flexible because a measurement model is not required at the FC and the FC has not to know the local agent measurement model and the network

spatial configuration at a given time step (the sensor positions are not needed at the FC). Moreover, the local control—based on the agent position, the measurement model, and the estimation covariance (as detailed in sub-Section IID)—is more robust to communication failures [25] because an agent can apply control using local estimates instead of fused estimates at the FC that are not available due to a missed communication [14].

The local agent sequential estimation is performed by a KF in which the coefficient dynamic is modeled by a linear state space equation shared by all the agents:

$$\mathbf{c}_{i,k} = \mathbf{F}_k \mathbf{c}_{i,k-1} + \mathbf{G}_k \mathbf{u}_k + \mathbf{n}_k, \tag{2}$$

where $\mathbf{F}_k$ is the state transition matrix, $\mathbf{u}_k$ is a P-dimensional column vector of exogenous forcing factor, weighted by the known $L \times P$ matrix $\mathbf{G}_k$, and $\mathbf{n}_k$ are Gaussian-distributed independent noise vectors with known covariance matrix $\mathbf{Q}_k = diag([\sigma_{1,k}^2, \ldots, \sigma_{L,k}^2]^T)$, where $\sigma_{j,k}^2$ is the variance of the jth coefficient, with $j = 1, \ldots, L$.

Assuming a network composed of N sensors, the ith sensor, for $i = 1, \ldots, N$, acquires at each time step a noisy measurement $y_{i,k}$ of the field. The ith sensor measurement equation can be expressed as follows:

$$y_{i,k} = \mathbf{h}_{i,k} \mathbf{c}_{i,k} + e_{i,k}, \tag{3}$$

where $\mathbf{h}_{i,k} = [\psi_1(\mathbf{r}_{i,k}), \ldots, \psi_L(\mathbf{r}_{i,k})]$ is the measurement vector and $\mathbf{r}_{i,k}$ is the position of the ith sensor at time step k. The scalar $e_{i,k}$ is a Gaussian uncorrelated random noise, independent from $\mathbf{n}_k$, with variance $[\mathbf{R}]_{i,k} = \rho_{i,k}^2$. Each sensor runs the KF prediction and update steps to provide the sequential estimate of the coefficient vector $\hat{\mathbf{c}}_{i,k}$ and its covariance matrix $\hat{\mathbf{C}}_{i,k}$ to the FC. The FC fuses the local information matrix, $\hat{\mathbf{D}}_{i,k} = \hat{\mathbf{C}}_{i,k}^{-1}$, and the local information vector $\hat{\mathbf{g}}_{i,k} = \hat{\mathbf{D}}_{i,k} \hat{\mathbf{c}}_{i,k}$ by a weighted sum:

$$\hat{\mathbf{g}}_k = \sum_{i=1}^{N} w_i \hat{\mathbf{g}}_{i,k}, \tag{4}$$

$$\hat{\mathbf{D}}_k = \sum_{i=1}^{N} w_i \hat{\mathbf{D}}_{i,k}, \tag{5}$$

and then retrieves the global coefficient vector as $\hat{\mathbf{c}}_k = \hat{\mathbf{D}}_k^{-1} \hat{\mathbf{g}}_k$ and its covariance matrix as $\hat{\mathbf{C}}_k = \hat{\mathbf{D}}_k^{-1}$. The FC broadcasts the global estimates to the sensors to update the local estimates with the global ones.

In principle, the dynamic equation as well as the measurement equation can be nonlinear. In this case, a nonlinear sequential filter like the unscented KF [26] can be used. In this work, only the linear case is considered. When the dynamic of the coefficients is unknown, (2) is used with $\mathbf{F}_k = \mathbf{I}_L$ and $\mathbf{G}_k = \mathbf{O}_{L \times P}$ ($\mathbf{I}_L$ is the $L \times L$ identity matrix and $\mathbf{O}_{L \times P}$ is the $L \times P$ matrix having all zero entries), and with $\sigma_{j,k}^2$ as free parameters that can be tuned to adjust the velocity at which the system adapts its estimate to the true dynamic of the coefficients [27]. The trade-off to be considered is between the filtering response of the system and the estimate residual error [27].

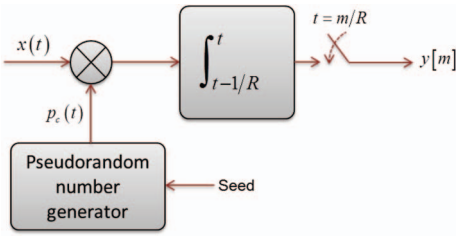

Fig. 2. RD scheme. Adapted from Tropp et al. [17].

B. Sensor Model and CS Measurement Equation

CS provides both the theoretical framework and the practical tools to efficiently approach the sampling and the reconstruction of sparse signals [28, 29]. The CS-sampling process is modeled by a linear system as follows:

$$\mathbf{y} = \Phi \mathbf{x}, \tag{6}$$

where $\mathbf{x} = [x_1, \ldots, x_W]^T$ is a sparse vector of W samples acquired at the Nyquist rate, Φ is an $M \times W$ sampling matrix, with $M < W$, and $\mathbf{y} = [y_1, \ldots, y_M]^T$ is a vector of M CS measurements. If the vector $\mathbf{x}$ has K unknown components different from zero, with $K \ll W$, CS theory states that x can be exactly recovered by minimizing its L_1-norm constrained by (6) from a number of CS measurements M proportional to $K \ln(W)$.

CS theory provides a way to sample more efficiently sparse signals where the sparsity is in a given linear transformed domain. This is typically carried out by developing cheap analog-sampling devices working at a lower sampling rate. A large part of research efforts in CS is devoted to the implementation of sampling schemes that can be modeled by (6) with random-sampling matrices. The RD device, proposed in [17] (see Fig. 2), consists in first modulating the analog input signal $x(t)$ with an analog random sequence $p_c(t)$ of impulses at Nyquist rate (the chip sequence) with amplitude that takes ± 1 equiprobable values. The modulator is followed by an integrator and a sample-and-hold device that works at a lower sampling rate than Nyquist. If the observation time is normalized to 1, the Nyquist rate is $1/W$, the integration is performed in the interval $[t, t - 1/M)$ and the sample-and-hold device works at a rate equal to $1/M$. At the end of the observation time, the device provides a vector of M samples given by (6). The sampling matrix Φ that models the RD in (6) can be decomposed as the product of two matrices, $\Phi = \mathbf{H}\Lambda$, where

$$\mathbf{H} = \begin{bmatrix} \overbrace{1\ 1\ 1}^{W/M} & 0 & 0 & 0 & 0 & \ldots & 0 & 0 & 0 \\ 0\ 0\ 0 & 1 & 1 & 1 & 0 & \ldots & 0 & 0 & 0 \\ 0\ 0\ 0 & \ldots & & & \ldots & 0 & 1 & 1 & 1 \end{bmatrix} \tag{7}$$

is a $M \times W$ matrix simulating the integration and $\Lambda = diag([p_0, \ldots, p_{W-1}]^T)$, with $p_j = \pm 1$, a sequence of equiprobable binary symbols simulating the chip sequence. Each row of $\mathbf{H}$ contains a sequence of 1s with a length of $B = W/M$ samples starting at the $(mB + 1)$th column, with $m = 0, \ldots, M - 1$.

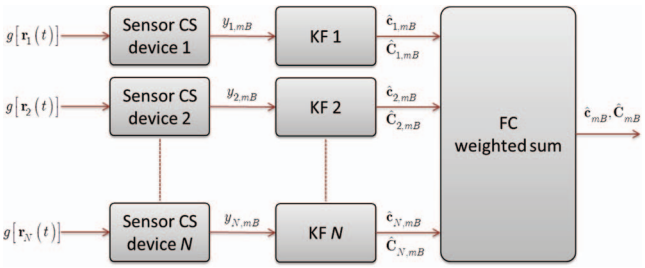

Fig. 3. Centralized KF estimation from CS samples of scalar field.

In this work, each sensor is equipped with a CS device like the RD. The local KF directly processes the CS samples working at a lower than Nyquist-sampling rate (see Fig. 3). In order to allow the KF to process such samples, the measurement equation, i.e., (3), has to be modified to properly model the RD-sampling process. If B is the CS block of Nyquist samples that are weighted by the chip sequence and then averaged, the CS sample at time $k = mB$ of the ith sensor is:

$$y_{i,mB} = \frac{1}{B}\mathbf{p}_{i,mB}^T \mathbf{H}_{i,mB}\mathbf{c}_{mB} + \frac{1}{B}\mathbf{p}_{i,mB}^T \mathbf{e}_{i,mB}, \tag{8}$$

where

$$\mathbf{H}_{i,mB} = \left[\mathbf{h}_{i,mB-B+1}^T, \ldots, \mathbf{h}_{i,mB-1}^T, \mathbf{h}_{i,mB}^T\right]^T \tag{9}$$

and

$$\mathbf{h}_{i,mB-b} = [\psi_1(\mathbf{r}_{i,mB-b}), \ldots, \psi_L(\mathbf{r}_{i,mB-b})] \tag{10}$$

With $b = B-1, \ldots, 0$. $\mathbf{p}_{i,mB} = [p_{i,mB,1}, \ldots, p_{i,mB,B}]^T$ is the chip random sequence of the ith sensor and $\mathbf{e}_{i,mB} = [e_{i,mB-B+1}, \ldots, e_{i,mB}]^T$ is the noise sequence in (3), for $k = mB - B + 1, \ldots, mB$. The local KF predicts the measurement using (8) and updates the coefficient estimate prediction $\hat{\mathbf{c}}_{i,mB|(m-1)B} = \mathbf{F}_{mB}\hat{\mathbf{c}}_{i,(m-1)B} + \mathbf{G}_{mB}\mathbf{u}_{mB}$ by using the innovation between the actual measurement and the predicted one. The final measurement equation is:

$$y_{i,mB} = \mathbf{q}_{i,mB}\mathbf{c}_{i,mB} + \varepsilon_{i,mB} \tag{11}$$

where

$$\mathbf{q}_{i,mB} = \frac{1}{B}\mathbf{p}_{i,mB}^T \mathbf{H}_{i,mB} \tag{12}$$

and $\varepsilon_{i,mB} = \mathbf{p}_{i,mB}^T \mathbf{e}_{i,mB}/B$, is a Gaussian random noise having the same variance of $e_{i,k}$ (this is due to the particular choice of the chip sequence).

C. SA-KF

In order to take advantage of the sparse structure of the coefficient vector, the local KF applies a further step after the measurement update that refines the coefficient estimation enforcing sparsity (see Fig. 4). The filter is inspired by the so-called SA-KF as proposed in [15, 16]. This filter substitutes the classical Kalman update step with a gradient descent iterative algorithm initialized by the predicted state vector estimate in order to minimize a

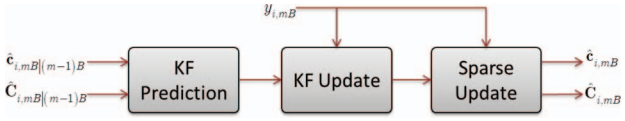

Fig. 4. KF with sparse refining scheme.

three-term functional that include the L_1-norm of the state vector. The approach followed here is similar to [15, 16] with the iterative minimization initialized by the state vector estimate updated by the classical Kalman update step. In particular, the refinement step consists in minimizing a cost function composed of three additive terms: 1) the square error between the coefficient $\mathbf{c}_{i,mB}$ and the Kalman estimate $\hat{\mathbf{c}}_{i,mB}$, weighted by $\hat{\mathbf{C}}_{i,mB}^{-1}$; 2) the square error between the measurement vector $y_{i,mB}$ and the predicted measurement $\mathbf{q}_{i,mB}\mathbf{c}_{i,mB}$; and 3) the L_1-norm of the coefficient vector, i.e., the term that promotes sparsity in the solution, weighted by a constant parameter λ_{SA} that controls the sparsity bias trade-off [15, 16].

The refined estimate of the coefficient vector is obtained by minimizing the following cost function:

$$\begin{aligned}\tilde{\mathbf{c}}_{i,mB} &= \arg\min_{\mathbf{c}_{mB}}[J_{SA}(\mathbf{c}_{i,mB})] \\ &= \arg\min_{\mathbf{c}_{mB}}\Big[\left\|\mathbf{c}_{i,mB} - \hat{\mathbf{c}}_{i,mB}\right\|_{\hat{\mathbf{C}}_{i,mB}^{-1}}^2 \\ &\quad + \left\|y_{i,mB} - \mathbf{q}_{i,mB}\mathbf{c}_{i,mB}\right\|_{R_{i,mB}^{-1}}^2 + \lambda_{SA}\left\|\mathbf{c}_{i,mB}\right\|_1\Big].\end{aligned} \tag{13}$$

Equation (13) is solved iteratively by a stochastic gradient descent algorithm. Given the coefficient state transition equation, i.e., (2), with $\mathbf{F}_k = \mathbf{I}_L$ and $\mathbf{G}_k = \mathbf{O}_{L\times P}$ and the measurement matrix (12), the gradient of the cost function in (13) can be written as:

$$\begin{aligned}\nabla J_{SA}(\mathbf{c}_{i,mB}) = 2[&-\hat{\mathbf{C}}_{i,mB}^{-1}(\mathbf{c}_{i,mB} - \hat{\mathbf{c}}_{i,mB}) \\ &- \mathbf{q}_{i,mB}^T R_{i,mB}^{-1}(y_{i,mB} - \mathbf{q}_{i,mB}\mathbf{c}_{i,mB}) + \lambda_{SA}\mathbf{1}_L]\end{aligned} \tag{14}$$

that is valid for positive coefficients for which the L_1-norm is differentiable.

The refined solution is found by iterating the following equation:

$$\tilde{\mathbf{c}}_{i,mB}(l+1) = \tilde{\mathbf{c}}_{i,mB}(l) - \gamma_{SA}\nabla J[\tilde{\mathbf{c}}_{i,mB}(l)], \tag{15}$$

where γ_{SA} is an update step size parameter, until the error between $\tilde{\mathbf{c}}_{mB}(l+1)$ and $\tilde{\mathbf{c}}_{mB}(l)$ is below a given threshold or after a maximum number of iterations. The iteration starts with the coefficient estimate at the output of the regular KF stage, i.e., $\tilde{\mathbf{c}}_{i,mB}(0) = \hat{\mathbf{c}}_{i,mB}$. The estimate can also be constrained; in case of nonnegativity constraints, for instance, the estimate (15) can be projected onto the nonnegative orthant as proposed in [15, 16].

In this work, a modification to the algorithm (13) is proposed in which the L_1-norm term is substituted by a smoothed approximation of the L_0-norm of the coefficient

vector [30]:

$$F_{\zeta_{SA}}(\mathbf{c}_{i,mB}) = L - \sum_{j=1}^{L} \exp(-c_{i,j,mB}^2/2\zeta_{SA}^2),$$
$$= L - \sum_{j=1}^{L} f_{\zeta_{SA}}(c_{i,j,mB}) \quad (16)$$

referred to as smoothed L_0-norm (SL_0-norm). The limit of (16) as ζ_{SA} approaches zero is the L_0-norm of the coefficient vector, i.e.,

$$\lim_{\zeta_{SA}\to 0} F_{\zeta_{SA}}(\mathbf{c}_{i,mB}) = \left\|\mathbf{c}_{i,mB}\right\|_0. \quad (17)$$

The SL_0-norm is a better approximation of the L_0-norm, and it is differentiable everywhere. Equation (16) can be included in the objective function (13) with a small ζ_{SA}, instead of the L_1-norm, and the resulting objective function can be minimized by using the gradient algorithm (15), with the gradient vector that is equal to:

$$\nabla F_{\zeta_{SA}}(\mathbf{c}_{i,mB}) = \frac{1}{\zeta_{SA}^2}[c_{i,1,mB} f_{\zeta_{SA}}(c_{i,1,mB}), \cdots, c_{i,L,mB} f_{\zeta_{SA}}(c_{i,L,mB})]^T. \quad (18)$$

The final estimate is then updated with the refined solution, i.e., $\hat{\mathbf{c}}_{i,mB} = \tilde{\mathbf{c}}_{i,mB}$, accepting the approximation of considering the covariance of the final estimate equal to the covariance at the output of the regular KF.

Several approaches to enforce sparsity in the KF have been proposed in the literature other than [15, 16], such as the one based on pseudomeasurement-norms and quasinorms as described in [31]. Section IV reports a comparison among the refining procedure proposed here, the classical SA-KF in [15, 16], and the pseudomeasurement approach in [31], showing that the first approach outperforms the others using the same number of iterations.

D. Network Control

Following [18], the local sensor control is given by updating the agent position in order to minimize the average covariance of the scalar field estimate at the time step $k+1$ with respect to the agent position. The field covariance is given by:

$$J = \int_A \Psi(\mathbf{r})\hat{\mathbf{C}}_{i,k+1}\Psi^T(\mathbf{r})dA, \quad (19)$$

where the integration is over the whole area of interest, with $A \in \mathbb{R}^2$ or $A \in \mathbb{R}^3$, in which the network of agents is constrained to operate. As in [18], the dynamical model of the ith agent is

$$\mathbf{r}_{i,k+1} = \mathbf{r}_{i,k} + \mathbf{f}_{i,k}, \quad (20)$$

where the control input $\mathbf{f}_{i,k}$ is implemented by a gradient control law as follows:

$$\mathbf{f}_{i,k} = -S\frac{\partial J}{\partial \mathbf{r}_i}|_{\mathbf{r}_i=\mathbf{r}_{i,k}}, \quad (21)$$

where

$$\frac{\partial J}{\partial \mathbf{r}_i} = \int_A \Psi(\mathbf{r})\frac{\partial \hat{\mathbf{C}}_{i,k+1}}{\partial \mathbf{r}_i}\Psi^T(\mathbf{r})dA, \quad (22)$$

and S is a constant gain.

According to [18], the nth component of the control input vector, with $n = 1, 2, 3$ in the 3D case, is given by an expression involving the state covariance matrix, the measurement matrix (10), and its gradient with respect to the agent position:

$$f_{i,n} = 2SR_i^{-1}\int_A \Psi(\mathbf{r})\hat{\mathbf{C}}_i\frac{\partial \mathbf{h}_i^T}{\partial r_{i,n}}(\mathbf{r}_i)\mathbf{h}_i(\mathbf{r}_i)\hat{\mathbf{C}}_i\Psi^T(\mathbf{r})dA, \quad (23)$$

where $\mathbf{h}_i(\mathbf{r}_i)$ is the agent measurement matrix (10) in the noncompressed domain, $\mathbf{r}_i = [r_{i,1}, r_{i,2}, r_{i,3}]$ and $R_i = \rho_i^2$. The time step index has been dropped for the sake of clarity. As shown in (23), the control law depends on the agent position through the measurement matrix. The derivatives of the measurement matrix with respect to $r_{i,n}$:

$$\frac{\partial \mathbf{h}_i}{\partial r_{i,n}} = \left[\frac{\partial \psi_1(\mathbf{r}_i)}{\partial r_{i,n}}, \ldots, \frac{\partial \psi_L(\mathbf{r}_i)}{\partial r_{i,n}}\right], \quad (24)$$

in case $\psi_j(\mathbf{r}_i)$ (with $j = 1, \ldots, L$) is a Gaussian radial basis function (RBF) with given mean vector $\bar{\mathbf{r}}_j$=$[r_{j,1}, r_{j,2}, r_{j,3}]$ and spreading parameter β_j, are given by:

$$\frac{\partial \psi_j(\mathbf{r}_i)}{\partial r_{i,n}} = -2\frac{r_{i,n} - \bar{r}_{j,n}}{\beta^2}\psi_j(\mathbf{r}_i), \quad (25)$$

with $\psi_j(\mathbf{r}_i) = \exp(-||\mathbf{r}_i - \bar{\mathbf{r}}_j||^2/\beta^2)$.

In the ideal centralized system, the control law can be applied by the ith agent at each time step k. The trajectory followed by the agent is the one that would allow it to optimally collect noncompressed measurements along the way. An approximation can be used by applying the control law at each $k = mB$ so that the first position within the next CS sampling window, at $k = mB + 1$, is the optimal one. This is the method used in the simulations to compare the centralized and the distributed consensus solutions as reported in Section IV. In both cases, the Kalman prediction of the covariance matrix, $\hat{\mathbf{C}}_{i,k+1|k}$, is actually used in (23) to calculate the control vector. In the case of a glider agent, in the consensus-based distributed system, the control is applied when the vehicle is at surface. The dynamic of the agents (20) is adapted, as specified in the subsection below, to model the behavior of an underwater glider vehicle having a constant speed (in the absence of sea current), a constrained vertical plane dynamic, and a waypoint guidance system. The control law in this case is used to optimally steer the direction of the vehicle on the horizontal plane toward the new waypoint.

E. Agent Kinematic Model: The Underwater Glider

In this work, underwater autonomous gliders [1] are considered to test the network architecture on simulated scenarios. Normally, in a typical mission setup, a glider

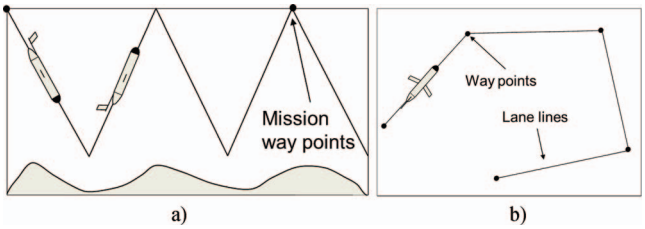

Fig. 5. Glider mission plan: (a) way points and lane lines in horizontal plane and (b) yo-yo trajectory in vertical plane.

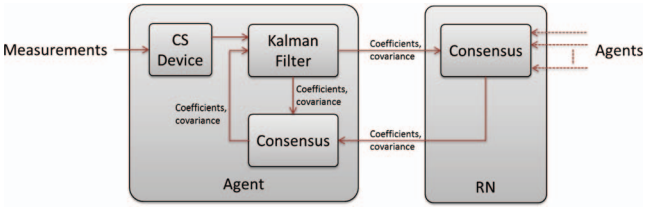

Fig. 6. Agent and RN structure.

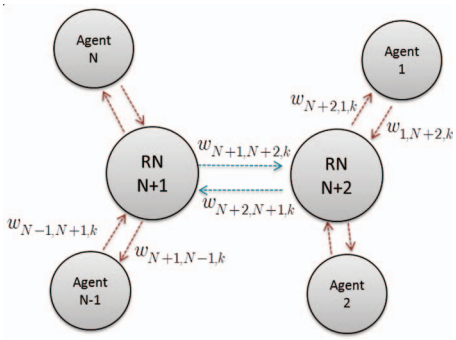

Fig. 7. Star network topology with time-varying link weights; example with two RNs.

moves through a 3D space following a saw tooth shape trajectory in the vertical plane and a waypoint list in the horizontal plane as in Fig. 5 to acquire measurements along the water column. The vehicle can be programmed to surface at each waypoint (typically every 1 to 3 h). The trajectory is composed of a certain number of dive/climb cycles in the interval between two waypoints. The data, collected along the water column, are stored and finally transmitted when at surface to a control room to be used later, e.g., in assimilation algorithms for ocean forecasting.

The glider dynamic model considered in this work assumes a constant velocity without water current disturbances (effects of water current will the subject of future investigations), constrained to follow a yo-yo trajectory in the vertical plane with given climbing and diving target depths [32]. The glider, in the absence of currents, navigates in the vertical plane along a yo-yo segment with a constant pitch angle ϕ. The control vector (21) is normalized and multiplied by the total glider speed V to take into account the constant speed constraint:

$$\tilde{\mathbf{f}}_{i,mB} = V\mathbf{f}_{i,mB} / \left\|\mathbf{f}_{i,mB}\right\| \tag{26}$$

Because the vehicle pitch is maintained constant during a dive/climb phase, the 2D horizontal plane components of (26) are used in the control law, at each glider surfacing when a waypoint is reached, to suboptimally steer the vehicle direction toward a new waypoint [14] to be reached after a given mean time, typically from 1 to 3 h.

III. DISTRIBUTED CONSENSUS ALGORITHM

In this section, the centralized model of Section II is modified to overcome the physical operational constraints of a typical underwater glider vehicle and to allow the deployment and the automatic control of a network of such vehicles in a decentralized way. The resulting network architecture has a switching topology [33] and is based on the consensus paradigm [34, 35] in which the information is diffused among the agents through the RNs, which act as an information gateway. Fig. 6 shows the basic structure of a single agent and a RN and the information flow between them.

A. Consensus Protocol

The following assumptions are made for the proposed network model. Agents can communicate with a RN at random instants. Agents cannot communicate among each other. Each agent sequentially estimates the coefficient vector by means of a SA-KF from local field measurements acquired by a CS device such as the RD (see the details in Section II).

Each agent updates its position by applying the control law and using the local prediction of the coefficient estimate covariance matrix. Agents communicating with the RNs transmit their local coefficient vector estimate and covariance; no field measurements are provided to the RNs. RNs distribute their estimate (coefficient vector estimate and covariance) to the connected agents and RN update their coefficient vector estimate and covariance by combining the local agent's estimates, when available, through the average consensus algorithm [10, 11] or propagates the previous estimate if no agents are connected. Agents connected to RNs update their local estimates (coefficient vector and covariance) by using RN estimates through average consensus.

The protocol allows the global information to intermittently flow into the network through RNs with a collaborative behavior among the agents who emerge above the sea surface to start the communication. Realistic numerical simulations show that all local agent estimates and RN estimates statistically converge close to the true global coefficient vector (i.e., the network reaches a consensus).

The network of agents and RNs can be modeled as an undirected graph with a topology sketched in Fig. 7. The whole network has a set of $N+N_r$ nodes, $N \equiv \{1, 2, \ldots, N+N_r\}$, with $\{N, \ldots, N+N_r\}$ the

indices of the RNs, and an adjacency matrix given by:

$$\mathbf{A} = \begin{bmatrix} \overbrace{\begin{matrix} 1 & & \\ & 1 & \\ & & \ddots \end{matrix}}^{N} & \overbrace{\begin{matrix} 1 & 1 \\ 1 & 1 \\ \vdots & \vdots \end{matrix}}^{N_r} \\ \begin{matrix} 1 & 1 & 1 & \cdots \\ 1 & 1 & 1 & \cdots \end{matrix} & \begin{matrix} 1 & 1 \\ 1 & 1 \end{matrix} \end{bmatrix} \begin{matrix} \left.\vphantom{\begin{matrix} 1 \\ 1 \\ \vdots \end{matrix}}\right\} N \\ \left.\vphantom{\begin{matrix} 1 \\ 1 \end{matrix}}\right\} N_r \end{matrix}, \tag{27}$$

which defines the set of all possible graph edges $\varepsilon \equiv \{(i,l)|A_{i,l} = 1, i, l \in \mathrm{N}\}$, with $A_{i,l}$ the ith row and lth column element of $\mathbf{A}$. Actually, the structure of the network is dynamic, i.e., at each time step k, there is a subset $\varepsilon_k \subseteq \varepsilon$ of edges that are active, where an edge $(i,l) \in \varepsilon_k$, with $i, l \in \mathrm{N}$, is active if node i can communicate with node l. At each $k = mB$, the consensus algorithm is applied to the local estimates of the information matrices $\hat{\mathbf{D}}_{i,mB} = \hat{\mathbf{C}}_{i,mB}^{-1}$ and the information vectors $\hat{\mathbf{g}}_{i,mB} = \hat{\mathbf{D}}_{i,mB}\hat{\mathbf{c}}_{i,mB}$ at each node, including the RN(s):

$$\hat{\mathbf{g}}_{i,mB} = \sum_{l \in \mathrm{N}_{i,mB}} w_{i,l,mB}\hat{\mathbf{g}}_{l,mB}, \tag{28}$$

$$\hat{\mathbf{D}}_{i,mB} = \sum_{l \in \mathrm{N}_{i,mB}} w_{i,l,mB}\hat{\mathbf{D}}_{l,mB}, \tag{29}$$

where $\mathrm{N}_{i,mB}$ is the set of node neighbors of the ith node (the node i is included in the set) at time step $k = mB$ and $w_{i,l,mB}$ are weighting parameters. Once the consensus has been applied, the updated coefficient estimate and the associated covariance for the ith node are $\hat{\mathbf{c}}_{i,mB} = \hat{\mathbf{D}}_{i,mB}^{-1}\hat{\mathbf{g}}_{i,mB}$ and $\hat{\mathbf{C}}_{i,mB} = \hat{\mathbf{D}}_{i,mB}^{-1}$, respectively. The choice of the weights in the consensus update is crucial for guaranteeing certain properties and asymptotic convergence. In particular, in this work, the Metropolis weights are considered:

$$w_{i,l,mB} = \begin{cases} 1/[1 + \max(d_{i,mB}, d_{l,mB})] & (i,l) \in \varepsilon_{mB} \\ 1 - \displaystyle\sum_{l \in \mathrm{N}_{i,mB} \setminus i} w_{i,l,mB} & i = l \\ 0 & \text{otherwise} \end{cases} \tag{30}$$

with $d_{i,mB} = |\mathrm{N}_{i,mB}|$ the cardinality of $\mathrm{N}_{i,mB}$. This choice is average preserving, and for certain problems of distributed consensus, it provides asymptotic convergence to a global solution under mild conditions on the sequence of sets of active edges ε_k.

In the case of a network of underwater gliders, the ith field sensor applies consensus if it is connected to a RN, when at surface, after having reached a waypoint. Define the time step at which the ith sensor reaches the wth waypoint at surface as $k_{i,w} = m_{i,w}B$. The sensor and the connected RN exchange their current estimates to each other (coefficient vector and associated covariance) and locally apply the consensus algorithm. The communication is through a radio or a satellite link. The glider calculates the correction to the navigation heading to point to the next waypoint according to the control law in sub-Section IID and then starts a new cycle of dive/climb phases. The next solution update is applied when the glider reaches the next waypoint at $k_{i,w+1} = m_{i,w}B + \Delta_i$ with Δ_i a random variable with given statistical distribution. In this work, Δ_i is a uniform random variable with a given mean value, i.e., a preprogrammed glider mission parameter usually between 1 and 3 h, within a given interval, typically 15 to 30 min wide, in order to model the uncertainty due to environmental factors affecting the vehicle navigation (such as unknown water currents).

The consensus update phase in this context is completely asynchronous. With the given network topology, the direct communication between glider agents is not possible. However, sensors indirectly combine their estimates among each other through the RNs. The RNs allow the diffusion of the information through the network and the convergence of any local agent estimates to the global statistic.

IV. RESULTS

In this section, the system is tested by simulating a network of underwater glider vehicles carrying onboard a sensor for measuring environmental parameters, like the seawater temperature. In all tests, the network has one RN. Two simulated scenarios are considered. The first one is static and it includes a sparse field simulated as a sum of Gaussian RBFs with constant coefficients. The second is dynamic and it simulates a field by using the same RBFs as the previous scenario with slowly varying sinusoidal coefficients. Both scenarios are in 3D. Statistics of the network performance are estimated through Mont Carlo simulations. Finally, a realistic nonsparse test case is considered in which the true 3D field is provided by a seawater temperature forecast model. The test case duration is 7 days, and it can be considered as a realistic simulation of a glider network operation.

The three scenarios here considered allow testing the system under different conditions related to the characteristics of the spatial field, including dynamic and sparsity of the state vector $\mathbf{c}$. The results are indicative of the general performance of the system in case of:

1) static sparse fields,
2) dynamic sparse fields, and
3) dynamic compressible fields.

A. Case Study 1: Constant Coefficients

In the first test case, the true spatial field is modelled in 3D as the weighted sum of $K = 4$ Gaussian RBFs with different mean position vector and the same covariance matrix, $\mathbf{V} = 0.05\mathbf{I}_3$ ($\mathbf{I}_3$ being the 3×3 identity matrix). The RBF spread parameter is given in normalized coordinates (between 0 and 1). The true nonzero coefficients are constant in time and equal to $\mathbf{c}_{true} = [3, 6, 9, 14]^T$.

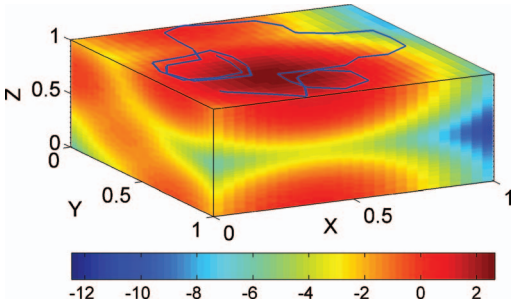

Fig. 8. True sparse field 3D view simulated as weighted sum of RBFs. Number of nonzero coefficients is $K = 4$ on total of $L = 64$ coefficients associated to 64 Gaussian RBFs distributed on regular grid. Intensity is in natural logarithmic scale. Blue line represents trajectory of agent projected on horizontal plane at $z = 1$.

The field is reconstructed on a $27 \times 27 \times 27$ 3D regular grid representing a spatial domain of 30×30 km along the x and y directions and 100 m along the vertical direction. Fig. 8 shows a 3D view of the true field and an example of the trajectory of an agent projected onto the horizontal plane (the 3D coordinates are normalized between 0 and 1 for convenience).

The sparse modeling of the field is obtained using a dictionary of 64 Gaussian RBFs with mean position vectors distributed on a regular $4 \times 4 \times 4$ 3D subgrid of the reconstruction grid and with the same known covariance matrix $\mathbf{V}$. The mean positions of the true field RBFs are distributed on four points of this subgrid (values are not included for brevity). Off-grid effects and different RBFs scale parameters are not considered in this work because they will be the subject for future investigations. The true field coefficient vector $\mathbf{c}$ is then a 64D sparse vector (whose entrances correspond to the lexicographical ordering of the RBFs mean position subgrid), with four components different from zero (the values being equal to the components of $\mathbf{c}_{true}$ above) and with support depending on the position of the mean of each true field RBF.

According to (2), the state equation for a single-agent KF is:

$$\mathbf{c}_k = \mathbf{I}_{64}\mathbf{c}_{k-1} + \mathbf{n}_k, \tag{31}$$

with the process noise covariance matrix set to $\mathbf{Q}_k = 0.003\mathbf{I}_{64}$ and where $\mathbf{I}_{64}$ is the 64×64 identity matrix. No exogenous inputs are considered. In this first test and in the next ones (see sub-Sections IVB and IVC), the true state model is considered unknown to the network. The process noise in (31) represents the uncertainty due to a not well-defined state equation the introduction of which allows tracking of slow time variations of the state vector in case of a model mismatch. The measurement equation of each agent is (11) with measurement noise equal to $R_k = 0.001$. The task of the distributed system is to estimate the state vector $\mathbf{c}$ (i.e., coefficient amplitudes and vector support) given the noisy measurements of the true field.

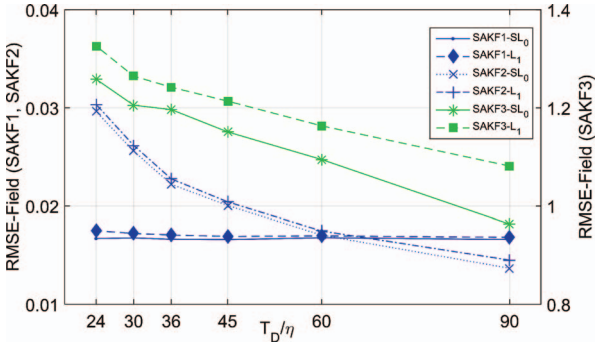

Fig. 9. Steady-state field RMSE. SA-KF algorithm comparison using 16 iterations. Performance averaged over 100 Monte Carlo simulations.

The network includes $N = 15$ glider agents with the same kinematic characteristics (the kinematic is constrained as in the glider case in Section III) and measurement sensors. The agent speed is 0.6 m/s, the pitch angle is $\phi = 26^\circ$, the sampling rate is $T = 6$ s, and the CS block length is $B = 5$ (i.e., one CS measurement every 30 sec and about 11 CS measurements along the water column in a single climb or dive phase). The chip sequence of the CS device is chosen at random according to subsection IIB. The SA-KF parameters are $\lambda_{SA} = 10^{-3}$, $\zeta_{SA} = 10^{-3}$, and $\gamma_{SA} = 10^{-5}$, while the number of iterations is 16. The time delay between adjacent surfacing/transmission phases of an agent is modelled as a uniform random variable $\Delta \in [\eta - \delta_s, \eta + \delta_s]$ to take into account random fluctuations due to unknown environmental conditions (sea current) affecting the agent navigation. The average delay η is typically between 1 to 3 h while in all the simulations δ_s is set to 15 min. The duration is $T_D = 72$ h.

Initially, the agents are placed uniformly at random in the considered domain, and the initial value of the coefficient estimates is supposed to be a Gaussian random variable with zero mean and 0.5 standard deviation. Performance statistics have been evaluated by carrying out 100 Monte Carlo runs. The performances are evaluated in terms of the steady-state field root mean square error (RMSE) as a function of the ratio $\gamma = T_D/\eta$ (the total number of connections in the observation period). The RMSE curve is compared against the ideal case of $\gamma \to +\infty$ and $\delta_s \to 0$, i.e., the centralized solution as in sub-Section IIA. The network has been simulated for different values of the mean transmission delay parameter $\eta \in \{0.8\text{h}, 1.2\text{h}, 1.6\text{h}, 2\text{h}, 2.4\text{h}, 3\text{h}\}$. The values of η are compatible with the kinematic and the track geometry of glider vehicles allowing at least one dive-climb cycle.

Fig. 9 shows the comparison in terms of steady-state field RMSE as a function of $\gamma = T_D/\eta$ among different SA-KFs as described in sub-Section IIC. In particular, the SAKF1 is the algorithm proposed in this work as a slight variant of the original SA-KF proposed in [15, 16], here referred to as SAKF2. A third implementation, here called SAKF3, is based on pseudomeasurement norms as proposed in [31]. The versions using both L_1 and SL_0 norms are also compared. The algorithms run using the

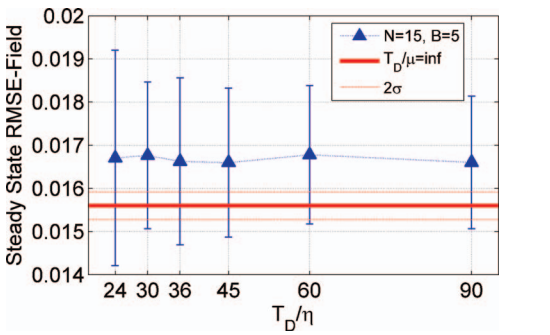

Fig. 10. Steady-state field RMSE at RN as function of $\gamma = T_D/\eta$ compared with centralized consensus solution. Constant coefficient case.

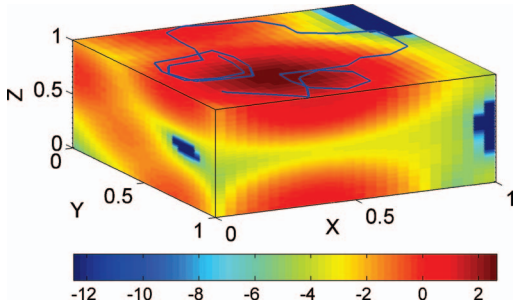

Fig. 11. Estimated field (natural logarithmic scale) at end of observation period with optimal trajectory for sensor 15 projected on horizontal plane.

same number of iterations, and the performance is averaged over 100 Monte Carlo simulations. The RMSE scale of SAKF1 and SAKF2 is reported on the left axis while the scale of the SAKF3 is reported on the right axis. The SAKF1 outperforms SAKF2 and SAKF3, with a slight improvement of the SL_0-norm version with respect to the L_1-norm one, for values of γ that are typical of a real glider mission setup (e.g., $\gamma = 45$). The SAKF1 and SAKF2 outperform the SAKF3 by two orders of magnitude. The SAKF1 RMSE is almost constant in the considered γ interval with a standard deviation that is about six times lower than the SAKF2, showing better solution stability ($\pm 2\sigma$ confidence levels are not reported in the graph for clarity). The SAKF1 has been chosen to run the simulations reported in the sequel of this section and in sub-Sections IVB and IVC.

Fig. 10 shows the steady-state field RMSE at the RN averaged over 100 Monte Carlo runs as function of $\gamma = T_D/\eta$ with 2σ bars (blue line) versus the RMSE of the centralized solution (in red). As expected, in the static case, the steady-state error does not depend significantly on γ within the range of values considered in the simulation. Its mean value is around 0.0167. The achieved average relative error is on the order of 2%.

Fig. 11 depicts the estimation of the field at the end of the observation period showing the good match with the true field in Fig. 8.

Fig. 12 provides the field RMSE versus time for $\gamma = 45$ ($\eta = 1.6$h), averaged over 100 Monte Carlo runs for both the RN and the sensors. After a transitory phase

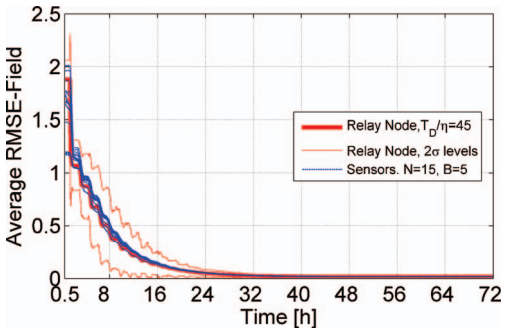

Fig. 12. Field RMSE (averaged over 100 Monte Carlo runs) versus time of RN and sensors for $\gamma = 45$.

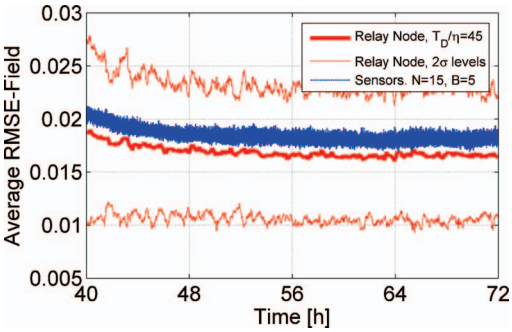

Fig. 13. Field RMSE (averaged over 100 Monte Carlo runs) versus time of RN and sensors for $\gamma = 45$. Zoom in of steady-state phase.

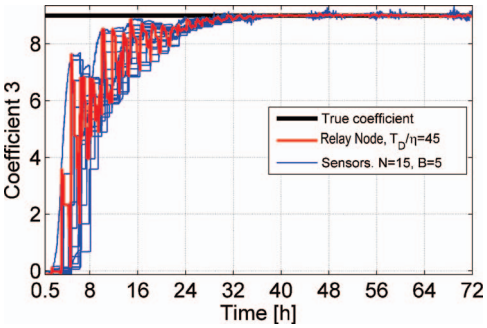

Fig. 14. Example of nonzero coefficient estimate versus time. Sensors and RN gradually reach consensus after about 48 h.

of about 48 h, the sensors (in blue) achieve a consensus, and the RMSE converge to the same value on average. The RMSE of the RN follows the same dynamic with 2σ confidence levels converging as well to a steady-state value.

Fig. 13 shows the steady-state phase of the graph in Fig. 12 confirming the convergence of the sensors and the RN RMSE. The RN average error slightly improves with respect to the mean of RMSE of sensors. The 2σ confidence intervals are close to each other, and therefore only the RN is reported.

Fig. 14 finally depicts the estimate of a nonzero coefficient versus time for the sensors and the RN ($\gamma = 45$). The sensors estimates are initially very different, producing oscillations in the RN estimate. The sensor and the RN estimates gradually converge to the true coefficient achieving consensus on average after about 48 h.

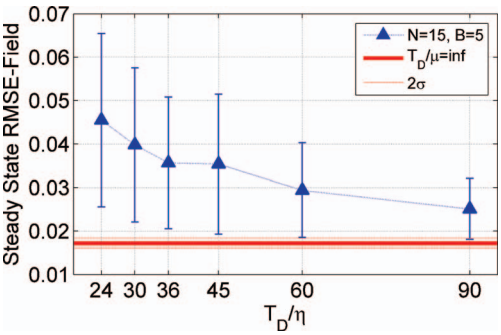

Fig. 15. Steady-state field RMSE at RN as function of $\gamma = T_D/\eta$ compared with centralized consensus solution. Sinusoidal coefficient case.

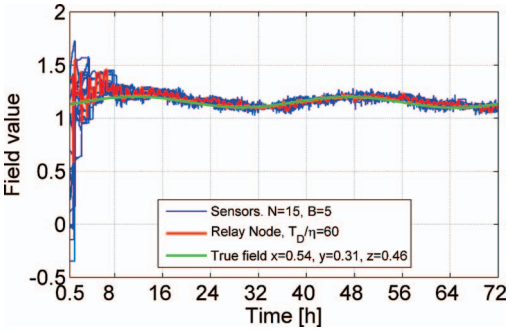

Fig. 16. Estimated field from sensors and FC at given position.

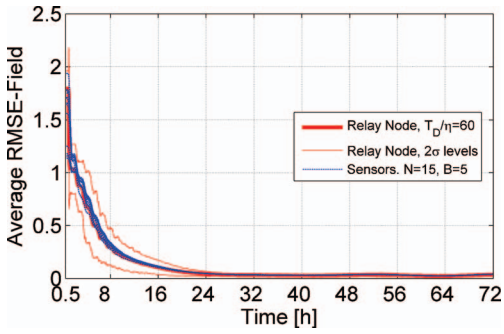

Fig. 17. Decentralized, sinusoidal coefficients, glider case. Temporal field RMSE.

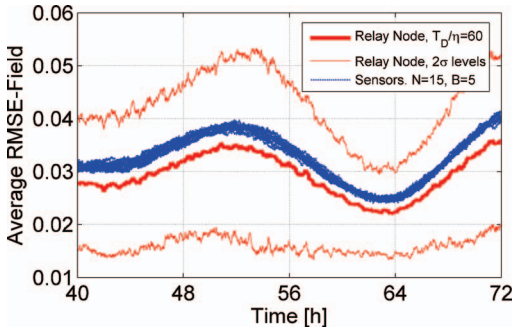

Fig. 18. Decentralized, sinusoidal coefficients, glider case. Temporal field RMSE. Steady-state phase.

B. Case Study 2: Sinusoidal Coefficients

In the second scenario, the field is modeled as in the previous case except for the coefficient amplitudes that are sinusoidal with the mean value as in the constant case and an amplitude that is 5% of the mean. The periods of the four sinusoidal components are set to $T_P \in \{6\text{h}, 7\text{h}, 8\text{h}, 9\text{h}\}$. The parameters of the simulation are the same as in the constant case, including the Gaussian RBF dictionary, agent model, Kalman state and measurement equations for each agent, number of agents, and statistical properties of the transmission delay. The average performance is evaluated over 100 Monte Carlo runs versus γ with the same time horizon T_D and η as in the previous case.

Fig. 15 shows the steady-state RMSE of the field for the RN (in blue) compared with the full centralized solution (in red). In contrast to the previous case, in a dynamic scenario, the RMSE is much more affected by the value of η.

In particular, the error at $\gamma = 24$ ($\eta = 3$h) is roughly twice the error at $\gamma = 90$ ($\eta = 0.8$h), asymptotically decreasing as γ varies between these two limits toward the ideal fully centralized solution. The average relative error is in general of the same order of magnitude as in the constant case.

Fig. 16 shows the field estimation of the RN (in red) and the sensors (in blue) versus time compared with the real field at a given position ($x = 0.54$, $y = 0.31$, and $z = 0.46$, in normalized coordinates). The network and the RN achieve a consensus, on average, after a transitory phase of about 24 h in which the local estimates are very different from each other. After the transitory phase, the network tries to track the true field variations with an error that depends on γ (in the example of Fig. 16, $\gamma = 60$, $\eta = 1.2$h).

Fig. 17 depicts the field RMSE versus time for the same $\gamma = 60$ ($\eta = 1.2$h), averaged over 100 Monte Carlo runs, for both the RN and the sensors. The sensors (in blue), after the transitory phase of 24 h, achieve a consensus with the RMSE converging to the same value on average. The RMSE of the RN (in red) follows the same dynamic with 2σ confidence levels converging as well to a steady state.

From Fig. 18, we get that, differently from the static case, the error in the steady phase presents a residual bounded oscillation around a constant value. As confirmed by Fig. 15, the mean and the amplitude of the residual oscillation decreases as γ increases (see both the mean value and the 2σ error bars), i.e., the network is improving the capability of tracking the real underlying field dynamic.

Finally, Fig. 19 shows the estimate of a nonzero coefficient versus time for the sensors and the RN (for the same case of $\gamma = 60$). As in the constant case, the sensors and the RN estimates, initially with different dynamics, gradually achieve a consensus (in roughly 24 h), and in the steady phase they track the true coefficient.

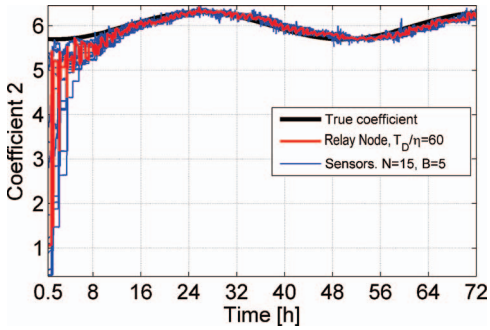

Fig. 19. Example of nonzero coefficient for sinusoidal case. Sensors and FC gradually reach consensus after 16 h and track coefficient variations.

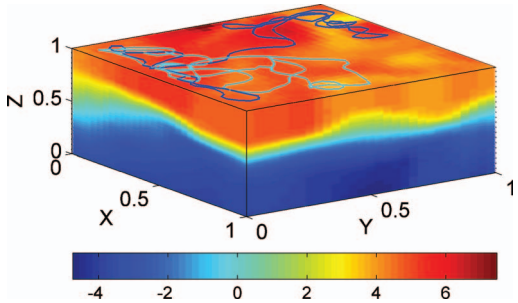

Fig. 20. Example of NCOM seawater temperature field variations at end of 7 days observation period and optimal trajectories projected on horizontal plane of two agents. Temperature variations are in degrees Centigrade around global mean.

C. NCOM Water Temperature Forecasts.

In a third scenario, the network task is the estimation of a nonsparse dynamic field. The true field is constructed by sequencing a series of consecutive 3D forecasts of seawater temperature (with 3 h sampling period) of the NCOM [20], spanning an observation period of 7 days. The model was provided by the Naval Research Laboratory–Stannis Space Centre, during the STO-CMRE 2011 Recognized Environmental Picture cruise trial (REP11) in the Mediterranean Sea. The data set used in the simulation represents a subvolume of about 60 by 60 km in the horizontal plane by 100 m along depth. The horizontal resolution is about 2 by 2 km. The initial depth levels (not regularly spaced) have been linearly interpolated between 0 and 100 m. The resulting regular data grid has a size of $30 \times 30 \times 30$ samples.

Fig. 20 shows an example of the true NCOM field at the end of the observation period. Without loss of generalities, the spatial/temporal mean of the field has been subtracted from the original data set. The system reconstructs the variations around that constant value.

The simulation setup is the same as in the previous cases except for the basis function dictionary that is of 343 Gaussian RBFs (i.e., the state coefficient vector $\mathbf{c}$ has 343 entries) arranged on a $7 \times 7 \times 7$ 3D regular subgrid of the original $30 \times 30 \times 30$ NCOM model grid. The RBF covariance matrix is $\mathbf{V} = 0.025\mathbf{I}_3$ constant for all the dictionary functions. The RBF spread parameter was

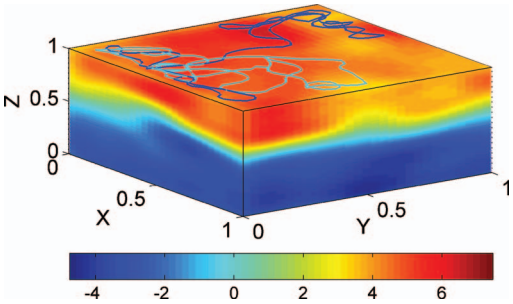

Fig. 21. Seawater temperature reconstructed field at end of observation period for NCOM case. Temperature variations are in degrees Centigrade around global mean.

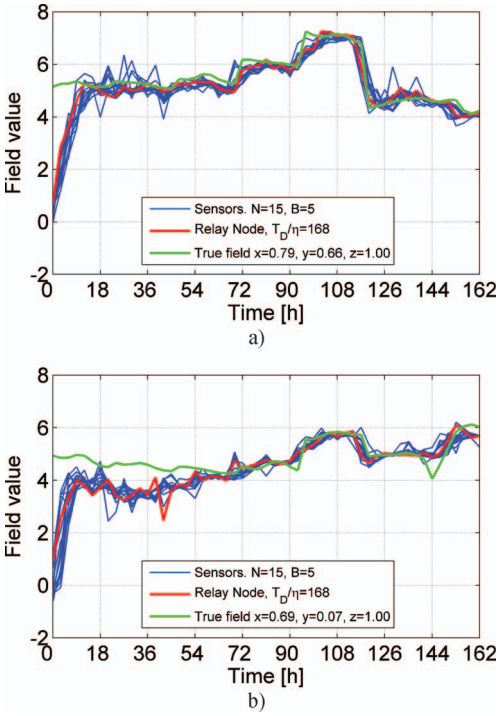

Fig. 22. Sensors and RN estimated field at given position subsampled every 3 h. (a) Transition phase duration of field estimates is about 18 h; after that estimates track true NCOM field variations. (b) Transition phase duration in this second case is about 72 h; after that estimates start to track true NCOM field variations more closely.

chosen empirically by roughly estimating the spatial scale of the main oceanographic features present in the data. The results are provided for a single realization because the scenario does not allow a series of Monte Carlo simulations in a reasonable time as in the previous simulated cases.

Fig. 21 presents the 3D view of the reconstruction of the field at the end of the observation period showing a good match with the true field in terms of the main oceanographic features both in the horizontal plane and along the vertical water column. The results are for a fleet of $N = 15$ gliders with $B = 5$ and $\eta = 1$h (i.e., $\gamma = 168$).

Fig. 22a shows the sensors and the RN field estimates versus time (subsampled every 3 h) for a given spatial position (with $x = 0.79$, $y = 0.66$, $z = 1.00$) compared

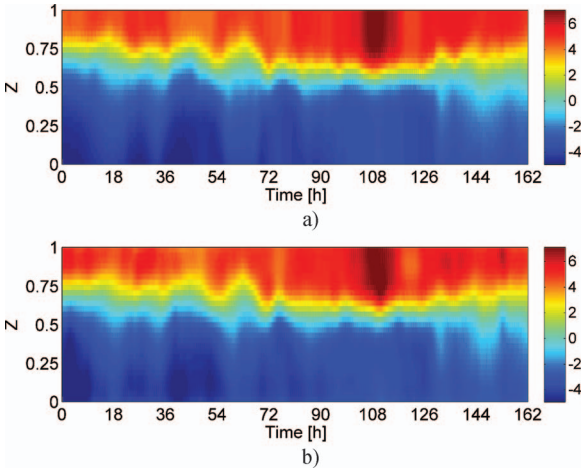

Fig. 23. (a) NCOM water temperature field vertical profile along agent 1 track (normalized z coordinates). (b) Estimated temperature field vertical profile along agent 1 track.

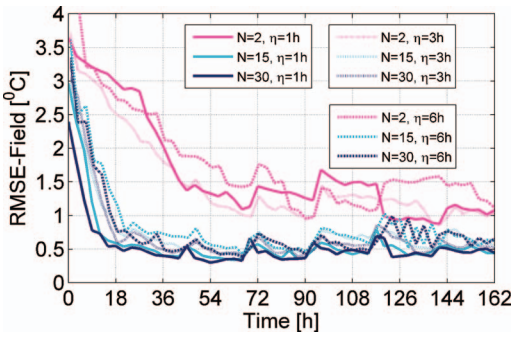

Fig. 24. Spatial field RMSE versus time for different values of N and η (3 h subsampling).

with the true field (in green). In this case, the system starts to track the field variations after a transition phase of about 18 h. In the case depicted in Fig. 22b (field versus time at position $x = 0.69$, $y = 0.07$, $z = 1.00$), the transition phase is longer, roughly 72 h, after that the sensors and the RN start to track the field variations more closely.

Fig. 23a shows the vertical profiles of the true NCOM field along the trajectory of agent 1 while Fig. 23b depicts the estimated profile by the same agent. The main oceanographic features are well resolved as well as the thermocline separating water masses with different characteristics.

Fig. 24 shows the spatial field RMSE versus time for different values of the N and η parameters. The graph can provide some indications on the best parameters to use in a real scenario, having the same time and spatial scale, and variability, in order to achieve the best possible performance at an affordable cost (in terms of number of sensors and number of transmissions in the observation period). In particular, the number of sensors significantly affects the error and the adaptation capability of the system for $N < 15$. After that limit, the RMSE value and the adaptation are almost stable (close to 0.5°C), and the η parameter does not significantly affect the performance. The spatial percentage error of the field is close to 10% after the transitory phase and for $N \geq 15$.

V. CONCLUSIONS

In this paper, an autonomous dynamic sensor network is proposed and tested on a scenario simulating the adaptive control of a fleet of autonomous underwater gliders. The task of the sensor network is to estimate 3D spatial scalar fields of ocean variables. The communication constraints and the sporadic asynchronous communications are the main operational limiting factors of these kinds of underwater networks. In order to cope with these issues, the proposed architecture manages in a distributed fashion both the field estimation and the agent control. Each agent performs the local estimation of the field statistics by a KF that processes local field measurements. The local estimates of an agent are updated, through an asynchronous consensus algorithm, exploiting the local estimates of the others. The information exchange is possible due to a subnetwork of RNs that communicate with the agents at the surface. The RNs apply consensus (asynchronously) to the local estimates of the agents and among them so as to provide an updated global field estimate that is exchanged with the agents themselves. In this way, all the nodes of the network converge on average to the global field statistics. This allows an agent to use global information to control its position in order to acquire field measurements in the most informative areas and adaptively track the field variations. The processing scheme can also take into account the spatial sparsity of the field by including at the agent level a SA-KF that refines the solution imposing L_0-norm sparsity constraints. Moreover, the local sampling scheme is based on a CS sampling device (such as the RD) to reduce the sampling rate and retain the field information. The CS samples are directly used in the local KF, on-line, without the need of reconstructing the measurement sequence at the original sampling rate.

The system has been tested on simulated scenarios both sparse and nonsparse. In the tests, the field is modeled by a dictionary of Gaussian RBFs. The first two scenarios include a constant and a dynamic sparse field while a third scenario simulates a glider fleet mission of 7 days using 3D time-varying seawater temperature data provided by the NCOM forecast model for a Mediterranean Sea area, in the framework of the REP11 experiment. For typical fleet operational parameters (i.e., 15 agents and 1–3 h surfacing period) and surveyed area size (30×30 or 60×60 km horizontally and 100 m vertically) the average performance achieved in terms of relative error at steady state is within 10%.

Future work can be directed in several ways. The on-line estimation of base functions unknown parameters, such as the mean and the covariance of Gaussian RBFs, is of particular importance in real applications. The problem is challenging because it involves nonlinearities that complicate the estimation step and also the agent control

law. Further work includes the investigation of the effects of the water current affecting agent navigation.

ACKNOWLEDGMENT

NCOM forecasts are provided by the US Naval Research Laboratory–Stennis Space Center (NRL-SSC) in the framework of the STO-CMRE REP11 experiment.

REFERENCES

[1] Schofield, O., Kohut, J., Aragon, D., Creed, L., Graver, J., Haldeman, C., Kerfoot, J., Roarty, H., Jones, C., Webb, D., and Glenn, S. M.
Slocum gliders: Robust and ready.
Journal of Field Robotics, **24**, 6 (2007), 1–14.

[2] Alvarez, A., Garau, B., and Caiti, A.
Combining networks of drifting profiling floats and gliders for adaptive sampling of the Ocean.
In *2007 IEEE International Conference on Robotics and Automation*, April 2007, 157–162.

[3] Fiorelli, E., Leonard, N. E., Bhatta, P., Paley, D. A., Bachmayer, R., and Fratantoni, D. M.
Multi-AUV control and adaptive sampling in Monterey Bay.
IEEE Journal of Oceanic Engineering, **31**, 4 (Oct. 2006), 935–948.

[4] Leonard, N. E., Paley, D. A., Lekien, F., Sepulchre, R., Fratantoni, D. M., and Davis, R. E.
Collective motion, sensor networks, and ocean sampling.
Proceedings of the IEEE, **95**, 1 (Jan. 2007), 48–74.

[5] Tu, S.-Y., and Sayed, A. H.
Mobile adaptive networks.
IEEE Journal of Selected Topics in Signal Processing, **5**, 4 (Aug. 2011), 649–664.

[6] Sayed, A.H., Tu, S.-Y., Chen, J., Zhao, X. and Towfic, Z. J.
Diffusion strategies for adaptation and learning over networks: an examination of distributed strategies and network behavior.
IEEE Signal Processing Magazine, **30**, 3 (May 2013), 155–171.

[7] Olfati-Saber, R., Fax, J. A., and Murray, R. M.
Consensus and cooperation in networked multi-agent systems.
Proceedings of the IEEE, **95**, 1 (Jan. 2007), 215–233.

[8] Olfati-Saber, R.
Flocking for multi-agent dynamic systems: algorithms and theory.
IEEE Transactions on Automatic Control, **51**, 3 (Mar. 2006), 401–420.

[9] Braca, P., Goldhahn, R., LePage, K., Marano, S., Matta V., and Willett, P.
Cognitive multistatic AUV networks.
Presented at the *Proceedings of the 17th International Conference on Information Fusion (FUSION 2014)*, Salamanca, Spain, 2014.

[10] Braca, P., Marano, S., Matta, V., and Willett, P.
Asymptotic optimality of running consensus in testing binary hypotheses.
IEEE Transactions on Signal Processing, **58**, 2 (Feb. 2010), 814–825.

[11] Braca, P., Marano, S., and Matta, V.
Enforcing consensus while monitoring the environment in wireless sensor networks.
IEEE Transactions on Signal Processing, **56**, 7 (Jul. 2008), 3375–3380.

[12] Kar, S., and Moura, J. M. F.
Consensus + innovations distributed inference over networks: cooperation and sensing in networked systems.
IEEE Signal Processing Magazine, **30**, 3 (May 2013), 99–109.

[13] Hine, R., Willcox, S., Hine, G., and Richardson, T.
The wave glider: A wave-powered autonomous marine vehicle.
In *OCEANS 2009, MTS/IEEE Biloxi - Marine Technology for Our Future: Global and Local Challenges*, Oct. 2009, 1–6.

[14] Grasso, R., Braca, P., Fortunati, S., Gini, F., and Greco, M. S.
Distributed underwater glider network with consensus Kalman filter for environmental field estimation.
Presented at the *Proceedings OCEANS 2015 MTS/IEEE*, Genova, Italy, 2015.

[15] Farahmand, S., Giannakis, G. B., Leus, G., and Tian, Z.
Sparsity-aware Kalman tracking of target signal strengths on a grid.
In *2011 Proceedings of the 14th International Conference on Information Fusion (FUSION)*, Jul. 2011, 1–6.

[16] Farahmand, S., Giannakis, G. B., Leus, G., and Tian, Z.
Tracking target signal strengths on a grid using sparsity.
EURASIP Journal on Advances in Signal Processing, Jan. 2014, doi: 10.1186/1687-6180-2014-7.

[17] Tropp, J.A., Laska, J. N., Duarte, M. F., Romberg, J. K., and Baraniuk, R. G.
Beyond Nyquist: Efficient sampling of sparse bandlimited signals.
IEEE Transactions on Information Theory, **56**, 1 (Jan. 2010), 520–544.

[18] Lynch, K. M., Schwartz, I. B., Yang, P., and Freeman, R. A.
Decentralized environmental modeling by mobile sensor networks.
IEEE Transactions on Robotics, **24**, 3 (Jun. 2008), 710–724.

[19] La, H. M., and Sheng, W.
Distributed sensor fusion for scalar field mapping using mobile sensor networks.
IEEE Transactions on Cybernetics, **43**, 2 (Apr. 2013), 766–778.

[20] Martin, P. J.
A description of the Navy Coastal Ocean Model Version 1.0.
NRL, Stennis Space Center, MS, NRL Rep. NRL/FR/7322-00-9962, 42 pp., 2000.

[21] Chang, K. C., Saha, R. K., and Bar-Shalom, Y.
On optimal track to-track fusion.
IEEE Transactions on Aerospace and Electronic Systems, **33**, 4 (Oct. 1997), 1271–1276.

[22] Tian, X., and Bar-Shalom, Y.
Track-to-track fusion configurations and association in a sliding window.
Journal of Advances in Information Fusion, **4**, 2 (Dec. 2009), 146–164.

[23] Uhlmann, J. K.
Covariance consistency methods for fault-tolerant distributed data fusion.
Information Fusion, **4** (2003), 201–215.

[24] Elad, M., and Yavneh, I.
A plurality of sparse representations is better than the sparsest one alone.
IEEE Transactions on Information Theory, **55**, 10 (Oct. 2009), 4701–4714.

[25] Brito, M. P., Smeed, D. A., and Griffiths, G.
Analysis of causation of loss of communication with marine autonomous systems: A probability tree approach.
Methods in Oceanography, **10** (Sep. 2014), 122–137.

[26] Julier, S. J., and Uhlmann, J. K.
Unscented filtering and nonlinear estimation.
Proceedings of the IEEE, **92**, 3 (Mar. 2004), 401–422.

[27] Merwe, van der R.
Sigma-point Kalman filters for probabilistic inference in dynamic state-space models.
Ph.D. dissertation, Oregon Health & Science University, April 2004.

[28] Donoho, D. L.
Compressed sensing.
IEEE Transactions on Information Theory, **52**, 4 (Apr. 2006), 1289–1306.

[29] Candes, E. J., Romberg, J., and Tao, T.
Stable signal recovery from incomplete and inaccurate measurement.
Communications on Pure and Applied Mathematics, **59**, 8 (Aug. 2006), 1207–1223.

[30] Mohimani, H., Babaie-Zadeh, M., and Jutten, C.
A fast approach for overcomplete sparse decomposition based on smoothed norm.
IEEE Transactions on Signal Processing, **57**, 1 (Jan. 2009), 289–301.

[31] Carmi, A., Gurfil, P., and Kanevsky, D.
Methods for sparse signal recovery using Kalman filtering pseudo-measurement norms and quasi-norms.
IEEE Transactions on Signal Processing, **58**, 4 (Apr. 2010), 2405–2409.

[32] Grasso, R., Cecchi, D., Cococcioni, M., Trees, C., Rixen, M., Alvarez, A., and Strode, C.
Model based decision support for underwater glider operation monitoring.
In *Proceedings OCEANS 2010 MTS/IEEE*, Seattle, WA, 1–8, 2010.

[33] Olfati-Saber, R., and Murray, R. M.
Consensus problems in networks of agents with switching topology and time-delays.
IEEE Transactions on Automatic Control, **49**, 9 (Sep. 2004), 1520–1533.

[34] Olfati-Saber, R.
Distributed Kalman filtering for sensor networks.
In *2007 46th IEEE Conference on Decision and Control*, Dec. 2007, 5492–5498.

[35] Olfati-Saber, R.
Distributed Kalman filter with embedded consensus filters.
In *44th IEEE Conference on Decision and Control, 2005, and 2005 European Control Conference, CDC-ECC '05*, Dec. 2005, 8179–8184.

Raffaele Grasso received the Laurea degree in telecommunication engineering from the University of Pisa, Pisa, Italy, in 1996, the Ph.D. degree in remote sensing from the University of Florence, Florence Italy, in 2000, and the Executive MBA from the LUISS Business School, Rome, Italy, in 2010. He is a scientist in the research department of the NATO Science & Technology Organization-Centre for Maritime Research and Experimentation (CMRE). His current research interests include statistical signal processing, compressive sensing, decision support systems, and optimal sensor network deployment and control, with applications in surveillance, environmental monitoring, and maritime operation planning. He is coauthor of more than 70 publications in international scientific journals and conference proceedings.

Paolo Braca (M'14) received the Laurea degree (summa cum laude) in electronic engineering and the Ph.D. degree (highest rank) in information engineering from the University of Salerno, Salerno, Italy, in 2006 and 2010, respectively. In 2009, he was a visiting scholar with the Department of Electrical and Computer Engineering, University of Connecticut, Storrs, CT. In 2010, he was a senior engineer with D'Appolonia S.p.A., Rome, Italy. In 2010–2011, he was a postdoctoral associate with the University of Salerno, Salerno, Italy. In October 2011, he joined the NATO Science & Technology Organization Centre for Maritime Research and Experimentation (CMRE) as a scientist with the research department. His research interest include statistical signal processing with emphasis on distributed inference, sensor networks, adaptation and learning over networks, multitarget/multisensor tracking, and data fusion. He is coauthor of more than 70 publications in international scientific journals and conference proceedings. Dr. Braca is currently an associate editor of the IEEE Signal Processing Magazine (E-Newsletter), the ISIF Journal of Advances in Information Fusion, and the EURASIP Journal of Advances in Signal Processing, and reviewer for several scientific journals and conferences. He is in the technical committee of the major international conferences in the field of signal processing and data fusion. He has been a coorganizer with Prof. P. K. Willett of the special session Multisensor Multitarget Tracking at the European Signal Processing Conference 2013. He was the recipient of the best student paper award (first runner-up) at the 12th Conference on Information Fusion in 2009.

Stefano Fortunati graduated in telecommunication engineering and received the Ph.D. degree at the University of Pisa, Italy, in 2008 and 2012, respectively. In 2012, he joined the Department of Ingegneria dell'Informazione of the University of Pisa, where he is currently working as temporary researcher. His general interests are in the areas of statistical signal processing, estimation, and detection theory. In particular, his research interests include robust estimation and detection theory, performance bounds, data fusion, target detection in non-Gaussian clutter, and CFAR techniques.

Fulvio Gini (Principal Investigator, Fellow IEEE) received the Doctor Engineer (cum laude) and the Research Doctor degrees in electronic engineering from the University of Pisa, Italy, in 1990 and 1995. respectively. In 1993, he joined the Department of Ingegneria dell'Informazione of the University of Pisa, where he become associate professor in 2000 and he is full professor since 2006. From July 1996 through January 1997, he was a visiting researcher at the Department of Electrical Engineering, University of Virginia, Charlottesville. He is an associate editor for the IEEE Transactions on Aerospace and Electronic Systems and for the Elsevier Signal Processing journal. He has been an associate editor for the Transactions on Signal Processing (2000–2006) and a member of the EURASIP JASP Editorial Board. He has been the editor-in-chief of the Hindawi International Journal on Navigation and Observation (IJNO). He is the area editor for the special issues of the IEEE Signal Processing Magazine. He was corecipient of the 2001 IEEE AES Society's Barry Carlton Award for Best Paper. He was recipient of the 2003 IEE Achievement Award for outstanding contribution in signal processing and of the 2003 IEEE AES Society Nathanson Award to the Young Engineer of the Year. He has been a member of the Signal Processing Theory and Methods (SPTM) Technical Committee of the IEEE Signal Processing Society and of the Sensor Array and Multichannel (SAM) TC for many years. He is a member of the board of directors of the EURASIP Society, the award chair (2006-2012) and the EURASIP president for the years 2013-2016. He was the technical cochair of the 2006 EURASIP Signal and Image Processing Conference (EUSIPCO), Florence, Italy, September 2006, of the 2008 Radar Conference, Rome, Italy, May 2008, and of the IEEE CAMSAP 2015 workshop, to be held in Cancun, Mexico, in December 2015. He was the general cochair of the 2nd Workshop on Cognitive Information Processing (CIP2010), of the IEEE ICASSP 2014, held in Florence in May 2014, and of the CoSeRa 2015 workshop on compressive sensing in radar, held in Pisa in June 2015. He was the guest coeditor of the special section of the Journal of the IEEE SP Society on Special Topics in Signal Processing on adaptive waveform design for agile sensing and communication (2007), guest editor of the special section of the IEEE Signal Processing Magazine on knowledge based systems for adaptive radar detection, tracking and classification (2006), guest coeditor of the two special issues of the EURASIP Signal Processing journal on new trends and findings in antenna array processing for radar (2004) and on advances in sensor array processing (in memory of Alex Gershman) (2013). He is coeditor and author of the book Knowledge Based Radar Detection, Tracking and Classification (2008) and of the book Waveform Diversity and Design (2012). His research interests include modeling and statistical analysis of radar clutter data, non-Gaussian signal detection and estimation, parameter estimation, and data extraction from multichannel interferometric SAR data. He authored or coauthored eight book chapters, about 120 journal papers, and more than 150 conference papers.

Maria S. Greco graduated in electronic engineering in 1993 and received the Ph.D. degree in telecommunication engineering in 1998, from University of Pisa, Italy. From December 1997 to May 1998 she joined the Georgia Tech Research Institute, Atlanta, GA as a visiting research scholar where she carried on research activity in the field of radar detection in non-Gaussian background. In 1993, she joined the Department of Information Engineering of the University of Pisa, where she is associate professor since December 2011. She has been an IEEE fellow since January 2011, and she was corecipient of the 2001 IEEE Aerospace and Electronic Systems Society's Barry Carlton Award for Best Paper and recipient of the 2008 Fred Nathanson Young Engineer of the Year award for contributions to signal processing, estimation, and detection theory. In May and June 2015, she visited as invited Professor the Université Paris-Sud, CentraleSupélec, Paris, France. She has been general-chair, technical program chair, and organizing committee member of many international conferences over the last 10 years. She is lead guest editor of the special issue on advanced signal processing for radar applications to appear on the IEEE Journal on Special Topics of Signal Processing, December 2015, she was guest coeditor of the special issue of the Journal of the IEEE Signal Processing Society on Special Topics in Signal Processing on adaptive waveform design for agile sensing and communication, published in June 2007, and lead guest editor of the special issue of International Journal of Navigation and Observation on modelling and processing of radar signals for Earth observation published in August 2008. She has been an associate editor of IET Proceedings–Sonar, Radar and Navigation, editor-in-chief of the IEEE Aerospace and Electronic Systems Magazine, member of the editorial board of the Springer Journal of Advances in Signal Processing (JASP), senior editorial board member of IEEE Journal on Selected Topics of Signal Processing (J-STSP), and member of the IEEE Signal Array Processing (SAM) Technical Committees. She has also been a member of the IEEE AES and IEEE SP Board of Governors and chair of the IEEE AESS Radar Panel. She has been as well SP Distinguished Lecturer for the years 2014–2015, AESS Distinguished Lecturer for the years 2015–2016, and member of the IEEE Fellow Committee. Maria is a coauthor of the tutorials entitled Radar Clutter Modeling, presented at the International Radar Conference (May 2005, Arlington, VA), Sea and Ground Radar Clutter Modeling presented at 2008 IEEE Radar Conference (May 2008, Rome, Italy) and at 2012 IEEE Radar Conference (May 2012, Atlanta, GA), coauthor of the tutorial RF and Digital Components for Highly-Integrated Low-Power Radar presented at the same conference, of the tutorial Recent Advances in Adaptive Radar Detection presented at the 2014 International Radar Conference (October 2014, Lille, France), and coauthor of the tutorial High Resolution Sea and Land Clutter Modeling and analysis, presented at the 2015 IEEE International Radar Conference (May 2015, Washington DC). Her general interests are in the areas of statistical signal processing, estimation, and detection theory. In particular, her research interests include clutter models, spectral analysis, coherent and incoherent detection in non-Gaussian clutter, CFAR techniques, radar waveform diversity, and bistatic/mustistatic active and passive radars. She coauthored many book chapters and more than 150 journal and conference papers.